polymers

MDPI

*Article*

# Fabrication and Characterization of PLA/PBAT Blends, Blend-Based Nanocomposites, and Their Supercritical Carbon Dioxide-Induced Foams

**Kartik Behera [1], Chien-Hsing Tsai [1], Xiang-Bo Liao [1] and Fang-Chyou Chiu [1,2,3,*]**

[1] Department of Chemical and Materials Engineering, Chang Gung University, Taoyuan 333, Taiwan; b.kartik1991@gmail.com (K.B.); a0970600013@gmail.com (C.-H.T.); brian2006tw@gmail.com (X.-B.L.)
[2] Department of General Dentistry, Chang Gung Memorial Hospital, Taoyuan 333, Taiwan
[3] Department of Chemical Engineering, Ming Chi University of Technology, New Taipei City 243, Taiwan
* Correspondence: maxson@mail.cgu.edu.tw

**Abstract:** In this study, a twin-screw extruder was used to fabricate poly(lactic acid) (PLA)/poly(butylene adipate-co-terephthalate) (PBAT) blends and blend-based nanocomposites with carbon nanotube (CNT) or nanocarbon black (CB) as nanofillers. The fabricated samples were subsequently treated with supercritical carbon dioxide ($scCO_2$) to fabricate the corresponding foams. Bi-phasic morphology and selective distribution of CNTs or CBs in the PBAT phase were observed in the blends/composites through scanning electron microscopy. After the $scCO_2$ treatment, the selective foaming of the PBAT phase in the prepared blends/composites was confirmed. The cellular structure of PBAT phase in $scCO_2$-treated blends is similar to the size/shape of PBAT domains in untreated blends or treated neat PBAT foam. The addition of CNTs or CBs in the blends led to a slight reduction in cell size of the foamed PBAT phase, demonstrating CNT/CB-induced cell nucleation. Differential scanning calorimetry (DSC) results showed that CNTs and CBs played as nucleating agents and increased the initial crystallization temperature up to 14 °C compared with neat PBAT for PBAT in different composites during cooling. The $scCO_2$ treatment induced the bimodal stability of PBAT crystals in different samples, which melted mainly in two temperature regions in DSC studies. Thermogravimetric analyses revealed that compared with parent blends, the addition of CNTs or CBs increased the temperature at 80 wt.% loss (degradation of PBAT portion) up to 6 °C. The electrical resistivity decreased by more than six orders of magnitude for certain CNT- or CB-added composites compared with the parent blends. The hardness of the blends slightly increased after forming the corresponding composites and then declined after the $scCO_2$ treatment.

**Keywords:** poly(lactic acid); poly(butylene adipate-co-terephthalate); nanocomposites; supercritical carbon dioxide; foams; physical properties

check for updates

**Citation:** Behera, K.; Tsai, C.-H.; Liao, X.-B.; Chiu, F.-C. Fabrication and Characterization of PLA/PBAT Blends, Blend-Based Nanocomposites, and Their Supercritical Carbon Dioxide-Induced Foams. *Polymers* **2024**, *16*, 1971. https://doi.org/10.3390/polym16141971

Academic Editor: Dimitrios Bikiaris

Received: 6 May 2024
Revised: 27 June 2024
Accepted: 5 July 2024
Published: 10 July 2024

**Copyright:** © 2024 by the authors. Licensee MDPI, Basel, Switzerland. This article is an open access article distributed under the terms and conditions of the Creative Commons Attribution (CC BY) license (https://creativecommons.org/licenses/by/4.0/).

## 1. Introduction

Poly(lactic acid) (PLA), a crucial bio-based and biodegradable polymer made from renewable sources, has gained great attention during the past two decades because of concerns about resource depletion and environmental pollution caused by petroleum-derived polymers [1,2]. The advantages of high stiffness, excellent transparency, good processability, low toxicity, and bio-compatibility offer PLA a wide range of applications in tissue engineering, medication administration, and food packaging [3–6]. However, the high cost, low ductility, and intrinsic brittleness of PLA limit its widespread adoption in applications requiring good toughness and lightweight compared with commercial polypropylene and polyethylene [2,6].

Foaming is a useful technique that offers numerous advantages and can decrease the weight of polymeric materials [7]. In contrast to their solid counterparts, microcellular-based plastic foams often possess not only lightweight but also superior impact strength

(IS), sound insulation, and heat insulation qualities. As a result, the foams are utilized in numerous industries, such as automotive, packaging, safety equipment, and construction [8,9]. The major challenge for foaming PLA lies in its notably low melt strength [10]. Cell coalescence and collapse readily occur due to the lack of robustness in cell walls during their expansion, resulting in the formation of open cells and an uneven distribution of cell sizes. To address this issue, previous works employed various effective methods, including chain extension, crosslinking, and blending, to enhance the foaming capability of PLA [11]. Blending is a cost-efficient and practically suitable approach for industrial-scale production. However, discovering a renewable method to toughen and maintain the rigidity of PLA as effectively as non-renewable methods remains challenging.

PLA has limited foamability and low toughness, which pose a significant obstacle to its widespread usage. Considerable efforts have been dedicated to improving the toughness of PLA [12–17]. Poly(butylene adipate-co-terephthalate) (PBAT) has emerged as one of the suitable choices to blend with PLA due to its favorable combination of biodegradability, high ductility, and impact resistance [18]. Wang et al. [19] investigated PLA/PBAT (60/40) blend, which achieved enhanced elongation at break (EB) (579.9%) and IS (29.6 kJ/m$^2$) through the incorporation of multifunctional epoxide as a reactive compatibilizer. Wu et al. [20] fabricated a highly durable PLA/PBAT/ethylenemethylacrylate-glycidyl methacrylate (EMA-GMA) (75/10/15) ternary blend by using reactive melt blending. The ternary blend exhibited an impressive notched IS of 61.9 kJ/m$^2$, nearly 13 times higher than that of the binary PLA/PBAT blend. The addition of 8 wt.% EMA-GMA increased EB to 320%, resulting in a 54.6% increase compared with the binary blend. Liu et al. [21] examined the effect of blending with PBAT on the crystallization behavior and foamability of PLA. Increasing PBAT content from 0 to 7 wt.% increased the PLA cell density from 2.01 $\times$ 10$^6$ to 1.74 $\times$ 10$^7$ cells/cm$^3$ and the expansion ratio from 4.87 to 10.94. Research has been conducted to enhance the thermal, electrical, and mechanical properties of polymers/blends by incorporating minimal quantities of nanofillers [22–25]. Of the fillers investigated, carbon nanofillers have been identified as suitable materials for increasing the properties of polymer matrices. For example, carbon nanotubes (CNTs) have shown the potential to remarkably enhance the rigidity and electrical properties of polymers by forming nanocomposites at low loadings (approximately <3 wt.%) [22,24]. Soni et al. [26] reported that carbon nanofiller-based composites are extensively employed in supercapacitors, solar cells, fuel cells, energy storage systems, the automobile sector, the electronics industry, packaging, and electromagnetic interference shielding applications. Urquijo et al. [27] fabricated PLA/PBAT/CNT composites through melt mixing. The IS of the PLA/PBAT (60/40) blend increased by 155% in the presence of 3 wt.% CNTs. The electrical percolation threshold was achieved with 1.28 wt.% CNTs in the PLA/PBAT blend. These findings highlight the incorporation of CNTs into PLA/PBAT blends, prompting further investigation into enhancing PLA foam properties through similar approaches.

Limited research has been undertaken to enhance the properties of PLA foams. Najafi et al. [28] investigated the impacts of long-chain branched (LCB) structure and adding organoclay on PLA foaming and determined the resultant mechanical properties. The incorporation of clay increased the crystallinity of linear PLA but decreased the crystallinity of LCB-PLA. However, in the supercritical carbon dioxide ($scCO_2$)-induced LCB-PLA composite foams, a high clay content increased specific IS, which surpassed that of unfoamed specimens. LCB-PLA with 0.5 wt.% clay showed a 37% increase in specific impact resistance, from 13.9 to 19.1 (kJ m$^{-2}$)/(kg m$^{-3}$). Livi et al. [29] investigated PBAT/imidazolium- and phosphonium-treated clay nanocomposites prepared by melt blending. The fabricated samples were subsequently treated with $scCO_2$ to prepare foams. The loading of 2 wt.% of imidazolium-treated clay drastically reduced the cell size from 600 µm to 125 µm. Lee et al. [30] found that blending polyhydroxyalkanoate (PHA) and nano-fibrillated polytetrafluoroethylene (PTFE) with PLA improved the IS of the final foams. The specific IS of both unfoamed and foamed samples increased with higher loadings of PTFE and PHA. Li et al. [31] investigated an efficient and eco-friendly approach utilizing $scCO_2$ for foaming

to produce PLA/CNT nanocomposite foams. The storage modulus of the composites exhibited a three-order-of-magnitude increase compared with that of pure PLA. PLA/CNT foam with a high volume expansion ratio of 49.6 times was successfully produced at a transition temperature of 121 °C. PBAT nanocomposite foams are less studied. Given the promising results from various studies on enhancing PLA foams, scholars should explore the effects of CNTs on PLA/PBAT blend.

According to the literature, PLA/PBAT blends show potential in various applications of biopolymers. The effects of loading CNTs or carbon nanoblacks (CBs) on different properties of PLA/PBAT blends should be worthy of investigation and comparison. In this report, we used CNTs or CBs as nanofillers to prepare PLA/PBAT blend-based nanocomposites through melt mixing. A compatibilizer was not added to the blends and composites. The prepared samples were treated with $scCO_2$ to fabricate corresponding foams with selective foaming in the PBAT phase only. The phase morphology, fillers' dispersibility, crystallization/melting behavior, thermal stability, tensile properties, hardness, and electrical resistivity of $scCO_2$-untreated samples were thoroughly assessed and compared. The developed cellular structure, melting behavior, and hardness of $scCO_2$-treated samples were preliminarily characterized. This study presents a viable method to fabricate fully bio-based PLA blend/composite foams with partial cellular structure development for potential use in packaging and bio-medical industries.

## 2. Materials and Methods

### *2.1. Materials and Sample Preparation*

PLA (Luminy® L175), with a melt flow rate of 8 g/10 min at 210 °C/2.16 kg, manufactured by Total Corbion PLA (Gorinchem, Netherlands) was used. PBAT (Ecoflex® C1200), purchased from BASF Co., Ltd., Ludwigshafen, Germany, was the blend counterpart for PLA. Multi-walled CNTs (ICT030) were purchased from Golden Innovation Business Co. Taiwan; CNTs have purity >90%, an average diameter of around 60 nm, and a length of 1–30 μm and served as nanofiller for preparing PLA/PBAT blend-based nanocomposites. CBs (VXC-72) manufactured by Cabot Corporation (Boston, MA, USA) with a diameter of around 30 nm were used as another kind of nanofiller for nanocomposite preparation.

Neat components were dried in a vacuum oven at 70 °C for 24 h before being fed into a twin-screw extruder to prepare blend/composite samples according to the formulation listed in Table 1. The twin-screw extruder SHJ-20B (Nanjing Jieya Extrusion Equipment Co., Nanjing, China) was employed, and the mixing temperature was set at 130 °C–210 °C from the feeding zone to the die zone at a screw speed ca. 360 rpm. The extruded and then pelletized samples were followed by injection molding (V4-20SP-G, Multiplas Enterprise Co., Taoyuan, Taiwan) and compression molding (Gotech GT-7014, Gotech, Taichung, Taiwan) to prepare specimens for subsequent characterizations. Specimens with dimensions of 20 mm × 5 mm × 1 mm were used for one-step $scCO_2$ batch foaming experiments. The specimens were put into an autoclave, and the temperature/pressure ($scCO_2$) was adjusted to 100 °C/4000 psi. After soaking in a $scCO_2$ environment for 2 h, the pressure was quickly released (less than 5 s) to normal pressure. The soaked specimens were taken out from the autoclave to room temperature.

**Table 1.** Sample codes and formulation.

| Sample Code | Composition | Parts (wt.%) |
|---|---|---|
| PLA | PLA | 100 |
| PBAT | PBAT | 100 |
| L3B1 | PLA/PBAT | 75/25 |
| L1B1 | PLA/PBAT | 50/50 |
| L1B3 | PLA/PBAT | 25/75 |
| L3B1-T1 | PLA/PBAT/CNT | 75/25/1 * |
| L1B1-T1 | PLA/PBAT/CNT | 50/50/1 * |
| L1B3-T1 | PLA/PBAT/CNT | 25/75/1 * |
| L3B1-B1 | PLA/PBAT/CB | 75/25/1 * |
| L1B1-B1 | PLA/PBAT/CB | 50/50/1 * |
| L1B3-B1 | PLA/PBAT/CB | 25/75/1 * |

* phr: parts per hundred parts of resin.

### *2.2. Characterization*

Scanning electron microscopy (Hitachi S-3000N, Tokyo, Japan; Jeol JSM-7500F, Tokyo, Japan) was used to observe the phase morphology and fillers' dispersibility of the cryo-fractured section of the prepared samples. The samples were immersed in liquid nitrogen before being fractured. The crystallization/melting behavior of PLA and PBAT in various samples was analyzed using a differential scanning calorimeter (TA DSC Q10, TA Instruments, New Castle, DE, USA). The $scCO_2$-untreated (unfoamed) samples were heated to 210 °C (molten state) at 20 °C/min and held for 3 min prior to being cooled to 20 °C at 10 °C/min for crystallization behavior study. The pre-cooled samples were subsequently subjected to 20 °C/min-heated to 210 °C for melting behavior investigation. The $scCO_2$-treated samples were directly 20 °C/min-heated from room temperature to 210 °C for melting behavior study without pre-cooling. Thermogravimetric analysis (TGA) experiments were carried out using a TA Q50 analyzer (TA Instruments, New Castle, DE, USA) under a nitrogen environment at a 10 °C/min heating rate. Tensile properties of dumbbell-shaped specimens (following ASTM D638) were measured at a crosshead speed of 10 mm/min by using a Gotech testing machine (AI-3000, Taiwan). The averaged values from five specimens of the same formulation were reported. The surface electrical resistivity of strip specimens was measured using resistivity meters (MCP-T700 and MCP-HT450, Mitsubishi Chemical Co., Tokyo, Japan) in a four-probe method. The measurements were performed four times for each specimen at a working voltage of 500 V and a duration of 10 s, and the average values were reported. Density was determined using a density meter (TWS-153E, MatsuHaku, Taichung, Taiwan). The porosity of the foamed samples was determined using the following equation [32]:

$$\text{Expansion ratio} = \frac{\rho_s}{\rho_F} \quad (1)$$

where $\rho_s$ is the sample density before foaming, and $\rho_F$ is the density of the corresponding foamed sample. Hardness was measured using a GS-702N TYPE D durometer (Teclock, Nagano, Japan).

## 3. Results and Discussion

### *3.1. Phase Morphology of Unfoamed Samples*

Figure 1a,b reveal the SEM images of neat PLA and PBAT, respectively. Both components show the typical rough texture of crystalline polymers. The SEM images of the blends are shown in Figure 1c–e, which exhibited bi-phasic morphology of immiscible characteristics. L3B1 and L1B3 (Figure 1c,e) exhibited sea-island morphology, with rounded minor component domains dispersed in the major component matrix. The dispersed domains had a broad distribution of diameter in the range of ca. 1–16 μm. Of the two blends, L1B3 had an average domain size of PLA larger than that of PBAT domains in L3B1 because of

the higher viscosity of PLA than that of PBAT under the mixing condition (PLA showed evidently a higher melting temperature than that of PBAT). Regarding L1B1 (Figure 1d), a co-continuous-like morphology was constructed by PBAT continuous phase and PLA(rich) continuous phase with small PBAT domain inclusion. The morphology of the PLA(rich) phase was similar to that of L3B1 but had a smaller PBAT domain size.

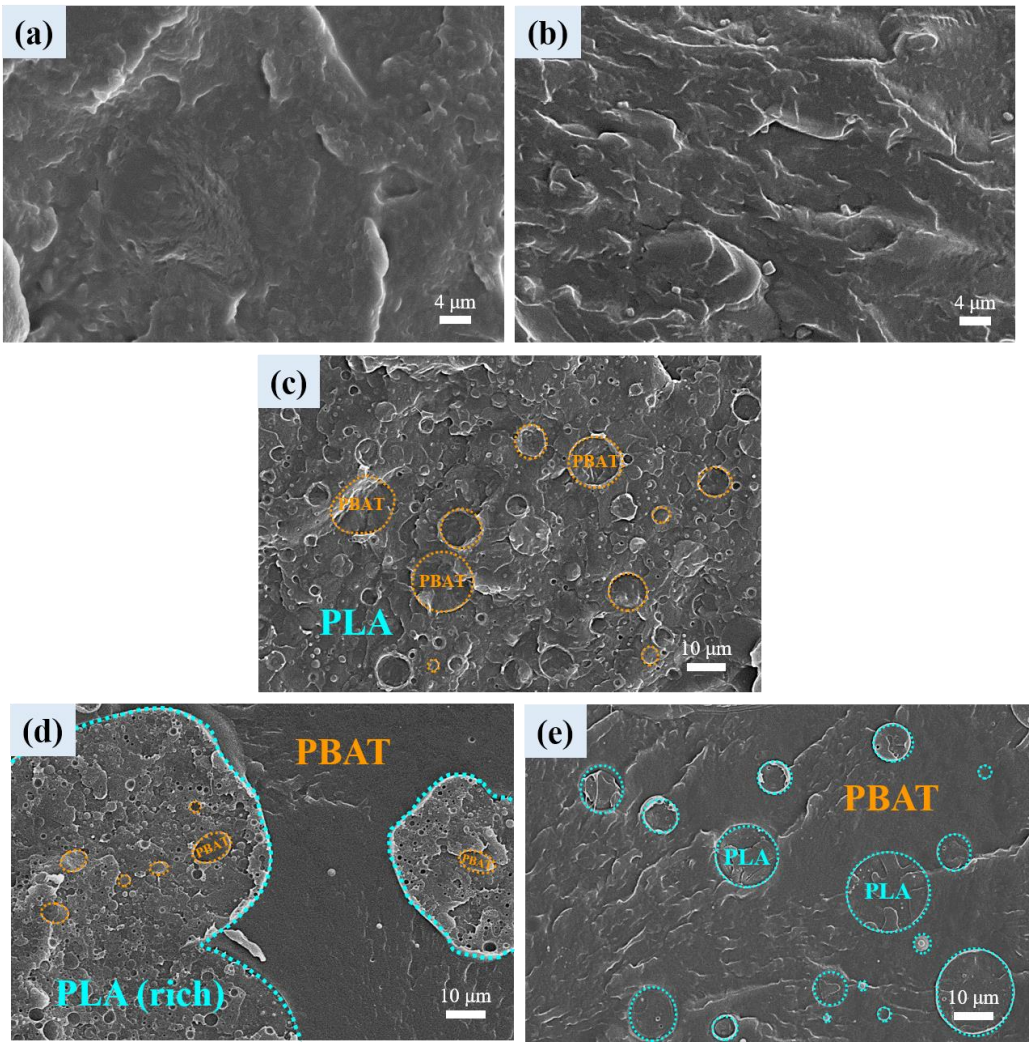



**Figure 1.** SEM images of (**a**) PLA, (**b**) PBAT, (**c**) L3B1, (**d**) L1B1, and (**e**) L1B3.

Figure 2 shows the high-magnification SEM images of representative blend-based composites with 1 phr CNTs or CBs inclusion to observe the dispersibility of added nanofillers. In L3B1-T1 and L3B1-C1 (Figure 2a,b), CNTs and CBs (arrowed) were selectively distributed in the dispersed PBAT domains (circled), which were hardly detected in the PLA matrix. The selective localization of CNTs in the PBAT phase of immiscible blends was reported previously [24], suggesting the superior affinity ($\pi$ electron) of carbon nanofillers to PBAT. For L1B1-T1 (Figure 2c,d), the added CNTs were likewise localized in the PBAT continuous phase and the dispersed PBAT domains within the PLA(rich) continuous phase. The dispersibility of CBs in the PBAT domains within the PLA(rich) continuous phase of L1B1-B1 and CNTs in the PBAT matrix of L1B3-T1 are illustrated in Figure 2e,f, respectively. Based on the SEM results of Figures 1 and 2, the L1B1 blend exhibited a (quasi)co-continuous phase morphology constructed by individual continuous PLA(rich) and PBAT phases, and the selective localization of carbon nanofillers in the PBAT phase of the nanocomposites was achieved.

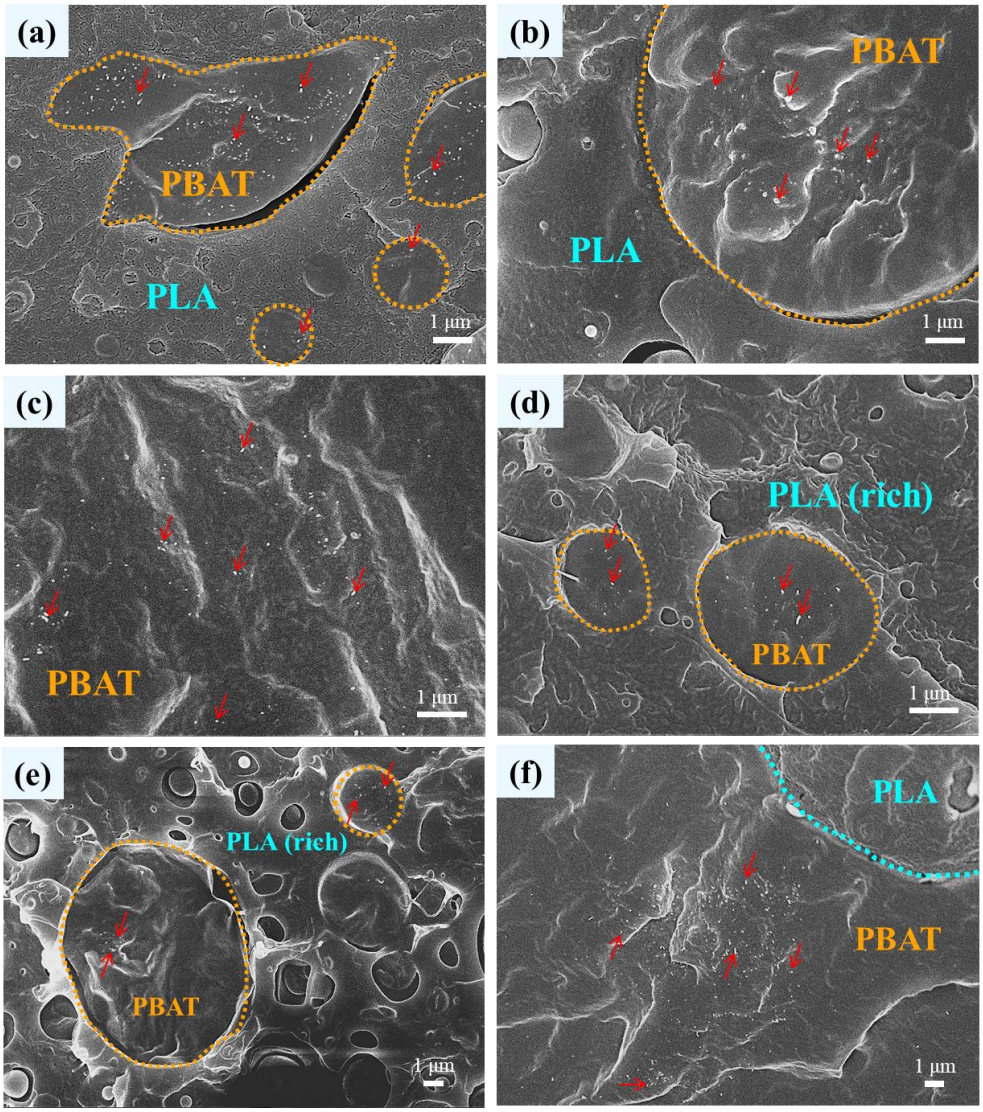



**Figure 2.** SEM micrographs of: (**a**) L3B1-T1, (**b**) L3B1-B1, (**c**) L1B1-T1(PBAT phase), (**d**) L1B1-T1(PLA-rich phase), (**e**) L1B1-B1(PLA-rich phase), and (**f**) L1B3-T1.

### *3.2. Crystallization and Melting Behavior of Unfoamed Samples*

The effects of forming blends and composites on the crystallization of PLA and PBAT were evaluated. Figure 3 depicts the DSC curves of various samples, which were 10 °C/min-cooled from the molten state. Figure 3a denotes the crystallization peak temperatures ($T_{Lc}$ and $T_{Bc}$) of neat PLA and neat PBAT, which were 88.6 °C and 92.0 °C, respectively. For the three blends shown in Figure 3b–d, only one exothermic peak was displayed, which seemed to be the superposition of the individual crystallization of PLA and PBAT. The exothermic enthalpy varied with the composition of the blend, showing a higher value with increasing PBAT content. A limited effect was observed on the crystallization of PLA and PBAT after forming the immiscible blends. Regarding the CNT- or CB-added composites, the merged single exotherm in the corresponding blends evolved into partially overlapped exotherms, which had a high-temperature exotherm. The intensity of the high-temperature exotherm increased with increasing PBAT content, demonstrating that the exotherm was associated with the crystallization of PBAT. The appearance of the high-temperature PBAT exotherm clearly indicated the nucleation effect of CNT/CB on PBAT crystallization, resulting from the selective localization of CNTs or CBs in the PBAT phase. The nucleation effect of CNTs for PLA and PBAT was previously reported [14,33]. The initial crystallization temperature ($T_i$, arrowed) in CNT-added composites was higher than that in corresponding CB-added

composites, suggesting that CNT had a superior heterogeneous nucleation effect to CB on facilitating PBAT crystallization. The $T_i$ of neat PBAT evidently increased from 114.3 °C to 128.3 °C in L1B3-T1. Regarding the crystallization temperature (peak position) of PLA, it did not vary after the addition of CNTs or CBs. CNTs and CBs, which were hardly localized in the PLA phase, were responsible for the observation. The differences in aspect ratio and surface structure were the main factors for the different efficiencies of CNT and CB in facilitating PBAT crystallization. The measurable $T_i$, $T_{Lc}$, and $T_{Bc}$, with some estimated values from the partially overlapped exotherms of different samples, are compared in Table 2.

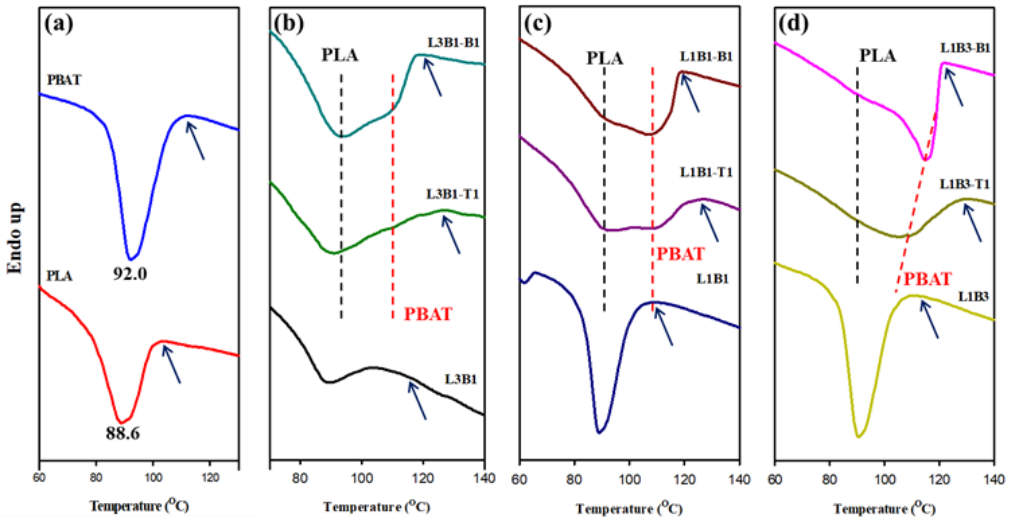



**Figure 3.** DSC 10 °C/min-cooled curves of (**a**) neat PLA and PBAT; (**b**) L3B1 and related composites; (**c**) L1B1 and related composites; and (**d**) L1B3 and related composites.

**Table 2.** DSC data of representative samples.

| Samples | Properties | | | | |
|---|---|---|---|---|---|
| | $T_i$ (°C) | $T_{Lc}$ (°C) | $T_{Bc}$ (°C) | $T_{Lm}$ (°C) | $T_{Bm}$ (°C) |
| PLA | 105.0 | 88.6 | - | 177.0 | - |
| PBAT | 114.3 | - | 92.0 | - | 131.3 |
| L3B1 | 107.9 | 88.5 | - | 176.3 | |
| L3B1-T1 | 127.0 | 91.2 | - | 178.0 | |
| L3B1-B1 | 122.3 | 93.5 | 109.0 | 178.0 | |
| L1B1 | 112.0 | 88.8 | - | 175.2 | 136.2 |
| L1B1-T1 | 126.6 | 92.2 | 107.9 | 174.6 | 141.8 |
| L1B1-B1 | 119.5 | 89.5 | 107.2 | 176.6 | 143.3 |
| L1B3 | 115.0 | 90.0 | - | 175.0 | 133.7 |
| L1B3-T1 | 128.3 | - | 107.6 | 175.5 | 141.6 |
| L1B3-B1 | 122.2 | - | 115.0 | 176.5 | 143.0 |

Figure 4 illustrates the DSC heating curves of 10 °C/min pre-cooled samples for evaluating the melting behavior of PLA and PBAT in different samples. In Figure 4a, neat PBAT exhibited a melting peak temperature ($T_{Bm}$) at 131.3 °C, and neat PLA showed a cold crystallization peak and melting peak temperature ($T_{Lm}$) at 102.7 °C and 177.0 °C, respectively. The typical shallow exotherm prior to PLA melting was due to the melting-recrystallization (annealing) of originally grown PLA crystals. For L3B1 and associated composites, the cold crystallization and melting of PLA were similar to those of neat PLA, whereas the melting of PBAT was hardly detected because of its low content. A slight increase in $T_{Lm}$ was observed in the composites. Regarding L1B1, L1B3, and their associated

composites (Figure 4b,c), the cold crystallization and melting of PLA again showed up, and the exothermic/endothermic enthalpy decreased as the PLA content decreased. The weak melting endotherm of PBAT was detected in L1B1- and L1B3-associated samples (Figure 4b′,c′), and the endotherm increased with increasing PBAT content. The determined $T_{Lm}$ and $T_{Bm}$ in different samples are summarized in Table 2. $T_{Bm}$ increased after forming the blend and further increased after adding either CNTs or CBs. The existence of PLA crystals and the added CNTs/CBs should have induced more stable PBAT crystals grown during pre-cooling. The increased $T_{Bm}$s in composites could be attributed to the decline in entropy change during crystal melting, thereby confining the effect caused by the dispersed CNTs or CBs.

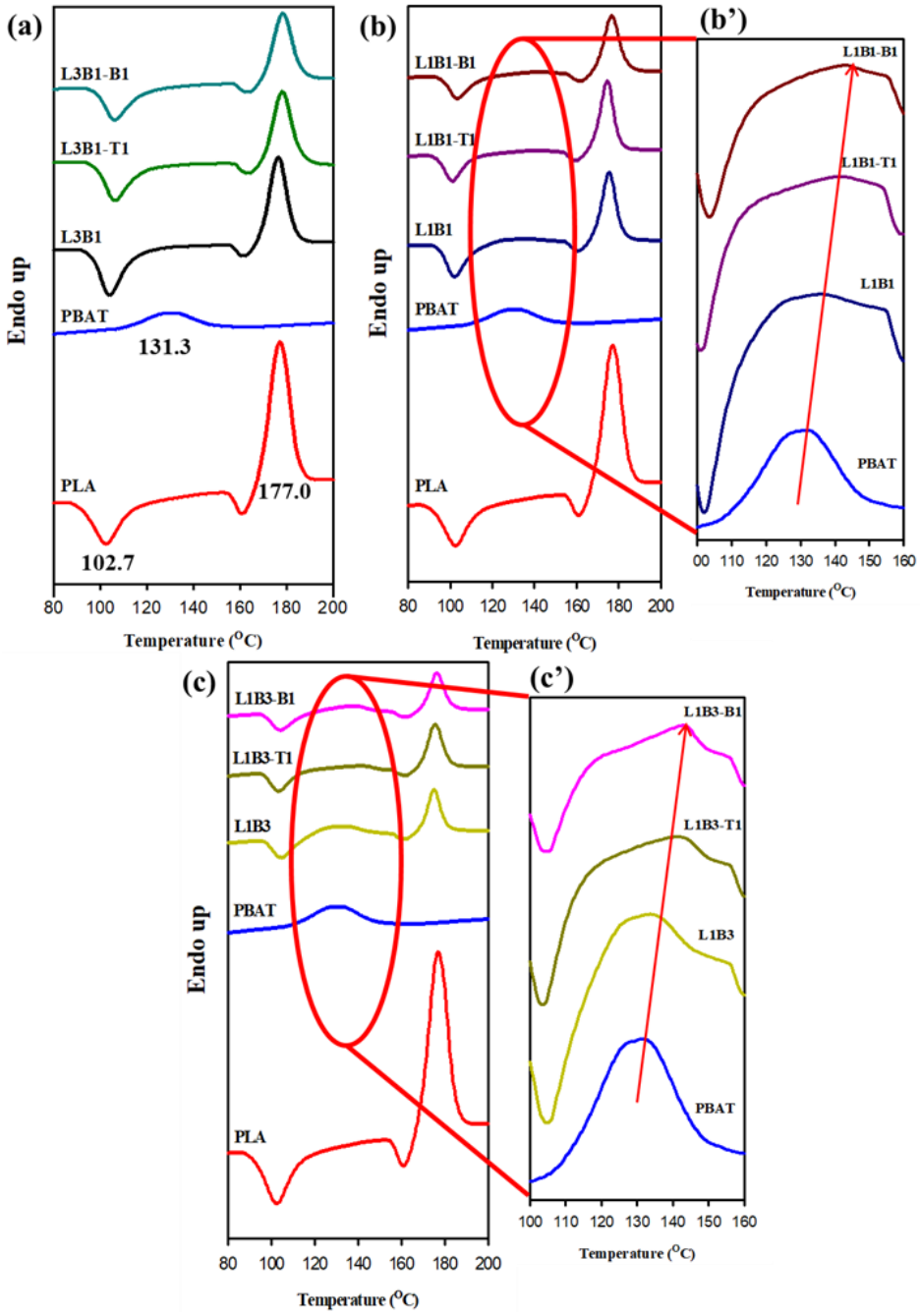



**Figure 4.** DSC 20 °C/min-heating curves of different samples after 10 °C/min pre-cooling: neat components and (**a**) L3B1 system, (**b**,**b′**) L1B1 system, and (**c**,**c′**) L1B3 system.

### *3.3. Thermal Stability of Unfoamed Samples*

The TGA-scanned curves of the samples are presented in Figure 5. PBAT exhibited thermal stability (degradation temperature) that was evidently higher than PLA, mainly due to its aromatic feature. The blends and composites exhibited two-staged degradation, corresponding to the degradation of individual PLA and PBAT. A higher content of PBAT in the blends/composites shifted the curves close to that of neat PBAT and led to a more evident second-stage PBAT degradation. The presence of CNTs or CBs hardly modified the first stage (PLA portion) degradation in the composites, whereas the second stage (PBAT portion) degradation discernibly shifted to higher temperatures in L3B1- and L1B1-based composites (arrowed). The stability improvement in the second stage degradation was attributed to the dispersion of CNTs or CBs in the PBAT phase. Behera et al. [33] reported that the thermal stability of the PBAT portion of the CNT-added composites was improved compared with that of the PBAT/HDPE blend. The excellent heat stability and radical scavenging function of carbon fillers are responsible for the observation. The L1B3-based composites hardly exhibited thermal stability improvement, which could be attributed to the lower dispersion density of CNT/CB in the PBAT phase compared with those of the corresponding L3B1- and L1B1-based composites. The degradation temperatures ($T_{d20}$ and $T_{d80}$) at 20% and 80% weight loss (representative degradation of PLA and PBAT, respectively) are compared in Table 3. $T_{d80}$ increased to 6 °C in L3B1-based composites compared with that in L3B1.

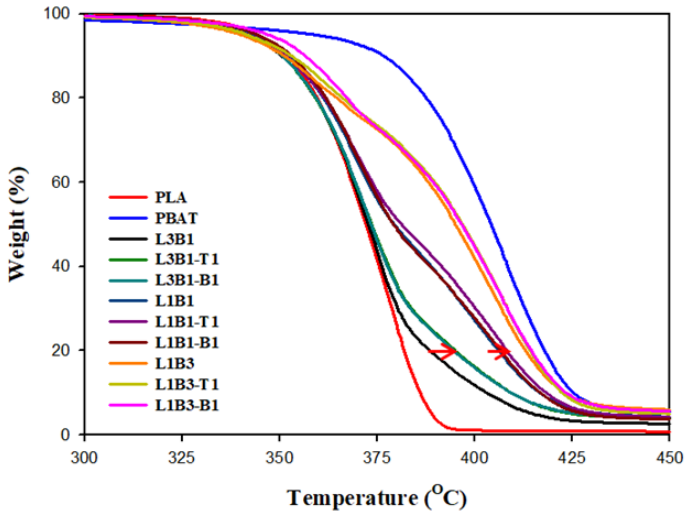



**Figure 5.** TGA curves of different samples heated at 10 °C/min in $N_2$.

**Table 3.** TGA data/tensile test data/electrical resistivity of unfoamed samples and cell size/porosity of foamed samples.

| Samples | Properties | | | | | | | |
|---|---|---|---|---|---|---|---|---|
| | $T_{20\%}$ (°C) | $T_{80\%}$ (°C) | TM (MPa) | TS (MPa) | EB (%) | Log ER (Ω-cm) | Cell Size (μm) | Porosity |
| PLA | 360 | 382 | 2287 ± 49 | 61.5 ± 0.7 | 3.3 ± 0.1 | >14 | - | - |
| PBAT | 388 | 418 | 105 ± 2 | 5.6 ± 0.4 | 9.2 ± 1.3 | >14 | 7.76 ± 2.12 | 0.48 |
| L3B1 | 359 | 389 | 1812 ± 44 | 43.7 ± 1.1 | 3.1 ± 0.1 | >14 | 2.72 ± 1.27 | 0.19 |
| L3B1-T1 | 359 | 395 | 1687 ± 39 | 32.2 ± 1.3 | 2.6 ± 0.2 | >14 | 3.44 ± 1.37 | 0.26 |
| L3B1-B1 | 359 | 395 | 1662 ± 40 | 35.4 ± 1.2 | 2.5 ± 0.2 | >14 | 2.98 ± 1.26 | 0.24 |
| L1B1 | 361 | 406 | 1025 ± 55 | 13.1 ± 1.1 | 2.0 ± 0.3 | >14 | 0.84 ± 0.45 * | 0.22 |
| L1B1-T1 | 362 | 409 | 802 ± 21 | 9.3 ± 1.2 | 1.9 ± 0.2 | 7.7 ± 0.5 | 0.53 ± 0.34 * | 0.19 |
| L1B1-B1 | 362 | 408 | 848 ± 38 | 8.9 ± 1.1 | 1.7 ± 0.2 | 7.8 ± 0.3 | 0.51 ± 0.35 * | 0.18 |
| L1B3 | 365 | 413 | 221 ± 5 | 7.5 ± 0.6 | 4.8 ± 0.5 | >14 | 5.25 ± 4.18 | 0.32 |
| L1B3-T1 | 366 | 414 | 229 ± 5 | 7.2 ± 0.7 | 5.0 ± 0.5 | 9.0 ± 0.7 | 3.32 ± 2.13 | 0.26 |
| L1B3-B1 | 367 | 415 | 244 ± 15 | 5.7 ± 0.4 | 4.0 ± 0.3 | 8.2 ± 0.2 | 4.30 ± 1.66 | 0.24 |

* in PLA(rich) phase.

### *3.4. Mechanical Property of Unfoamed Samples*

The tensile modulus (TM), tensile strength (TS), and elongation at break (EB) of the unfoamed samples were summarized in Table 3. Figure S1 depicts the typical stress-strain curves of the unfoamed samples. Neat PLA showed a TM value evidently higher than that of neat PBAT. TM of L3B1 and L1B1 were slightly higher than those (1741 MPa and 1196 MPa) calculated by the additivity rule. The (co)continuous phase played by PLA in L3B1/L1B1was responsible for the observation. L1B3 showed a TM much lower than the additivity rule calculated value (650 MPa) due to its immiscibility and the soft PBAT matrix. The TM values were adversely affected after adding CNTs or CBs in L3B1 and L1B1, which might be ascribed to the morphology modification and the location of CNTs/CBs in the PBAT domains. The L1B3-based composites, however, showed a slightly higher TM compared with L1B3 due to the localization of CNTs/CBs in the PBAT matrix. Regarding the TS of the samples, a similar formulation-dependent trend to that of TM results is observed. With increasing PLA content in the blends, TS gradually increased due to the higher TS of PLA compared with PBAT. However, the TS of the blends generally decreased after the loading of CNTs or CBs. Regarding the EB, PBAT had an evidently higher value than PLA. L3B1 and L1B1 exhibited lower EB values than those of neat components due to their immiscibility. L1B3 showed an EB slightly higher than that of PLA, attributed to the PBAT-dominated matrix. EB of the blends generally decreased after adding the CNTs or CBs.

### *3.5. Electrical Conductivity of Unfoamed Samples*

The surface electrical resistivity (ER) of the prepared samples is compared in Table 3. The ER values of neat components and the blends were higher than $10^{14}$ Ω-cm, demonstrating their insulating nature. For L3B1-T1 and L3B1-B1, ER remained higher than $10^{14}$ Ω-cm because the CNT- or CB-included PBAT phase played the dispersed domains surrounded by the insulating PLA phase. The percolation of CNTs or CBs was not achieved without forming the continuous PBAT phase (network). ER dropped more than six orders of magnitude for the L1B1- and L1B3-based composites. Jen et al. [25] reported that the loading of 3 phr CNTs reduced the ER by eight orders of magnitude for PLA/TPEE blend-based composites. The drastic ER drop suggested the formation of (quasi)connected CNT or CB network in the continuous PBAT phase of the composites. The continuous PBAT phase is revealed in Figures 1 and 2. (SEM images). The L1B1-based composites showed ER values slightly lower than the L1B3-based counterparts, attributed to the higher CNT or CB dispersion density in the PBAT phase of the L1B1 matrix than in the L1B3 matrix. After comparing the efficiency of adding CNTs and CBs in decreasing ER for the blend matrix, similar efficiency was obtained, though CNT had a higher aspect ratio than CB. The dispersibility and carbon purity of CNTs and CBs also played roles in affecting the electrical properties of the prepared composites.

### *3.6. Cellular Structure of Foamed Samples*

Figure 6 shows the internal structure of $scCO_2$-treated neat PLA and PBAT, as revealed by SEM. After the treatment at 100 °C/4000 psi for 2 h, PLA hardly exhibited cellular structure, whereas PBAT showed cellular structure of irregular/elongated shape. The cell rupture/collapse in PBAT was ascribed to its low melt strength of PBAT. PLA hardly grew cellular structure under the treated condition, so the prospective selective foaming of the PBAT portion in the phase-separated blends/composites was preliminarily assessed.

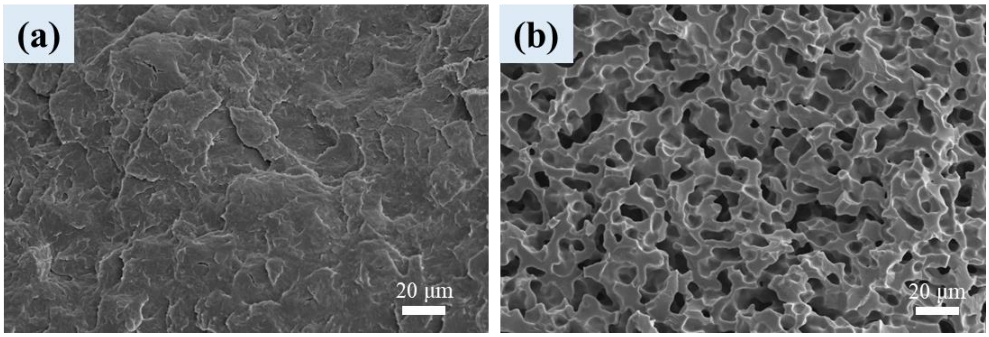



**Figure 6.** SEM images of $scCO_2$-treated (**a**) PLA and (**b**) PBAT.

Figure 7 shows the SEM internal structure of $scCO_2$-treated (foamed) L3B1 and L3B1-based composites. L3B1 (Figure 7a) showed a partially foamed structure with the size of the closed cell correlated with the dispersed PBAT domains in the unfoamed counterpart (Figure 1), indicating the occurrence of selective foaming in the PBAT phase. The rounded cells of various sizes were finely distributed in the PLA matrix. The presence of an un-foamable PLA matrix confined PBAT in small domains and inhibited the collapse/rupture of PBAT cells during foaming. Some large-sized cells were formed around the boundary between the PBAT and PLA phases. Some PBAT particles (arrowed) existed within the large-sized cells. The weak adhesion between PLA-PBAT phases led to cell nucleation and growth along the boundary. For the $scCO_2$-treated L3B1-based composites, a cellular structure similar to that of foamed L3B1 was observed (Figure 7b,c). The average size of PBAT cells in the composites was slightly larger than that in foamed L3B1, which might be attributed to the CNT/CB-caused aggregation in original PBAT domains prior to the $scCO_2$-treatment.

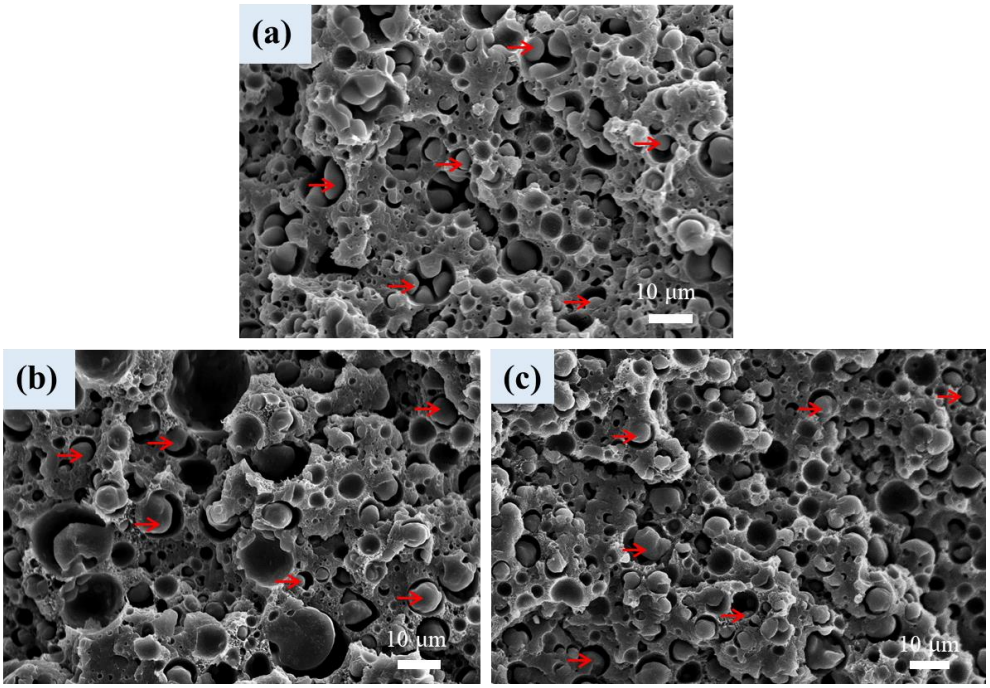



**Figure 7.** SEM cellular structure of (**a**) L3B1, (**b**) L3B1-T1, and (**c**) L3B1-B1.

As un-treated L1B1 exhibited (quasi)co-continuous PLA(rich) phase and PBAT phase (Figure 1), Figure 8a,b show the cellular structure in the individual PLA(rich) phase and PBAT phase of $scCO_2$-treated L1B1. In the PLA(rich) phase of Figure 8a, sphere-like PBAT cells with size/shape similar to the original un-foamed PBAT domains were developed.

Large PBAT cells with particle (arrowed) inclusion were also observed. Figure 8b shows the irregular/elongated shaped PBAT cells in the PBAT continuous phase, similar to those observed in $scCO_2$-treated neat PBAT. Figure 8c–f depicts the PBAT cellular structure in the individual PLA(rich) and PBAT continuous phases of L1B1-T1 and L1B1-C1 composites, respectively. The cellular structure was similar to those developed in the PLA(rich) phase and PBAT phase of parent L1B1 foam. The average PBAT cell size in the PLA(rich) phase was smaller in the composites compared with that in parent L1B1 foam, which was ascribed to CNT/CB-induced cell nucleation.

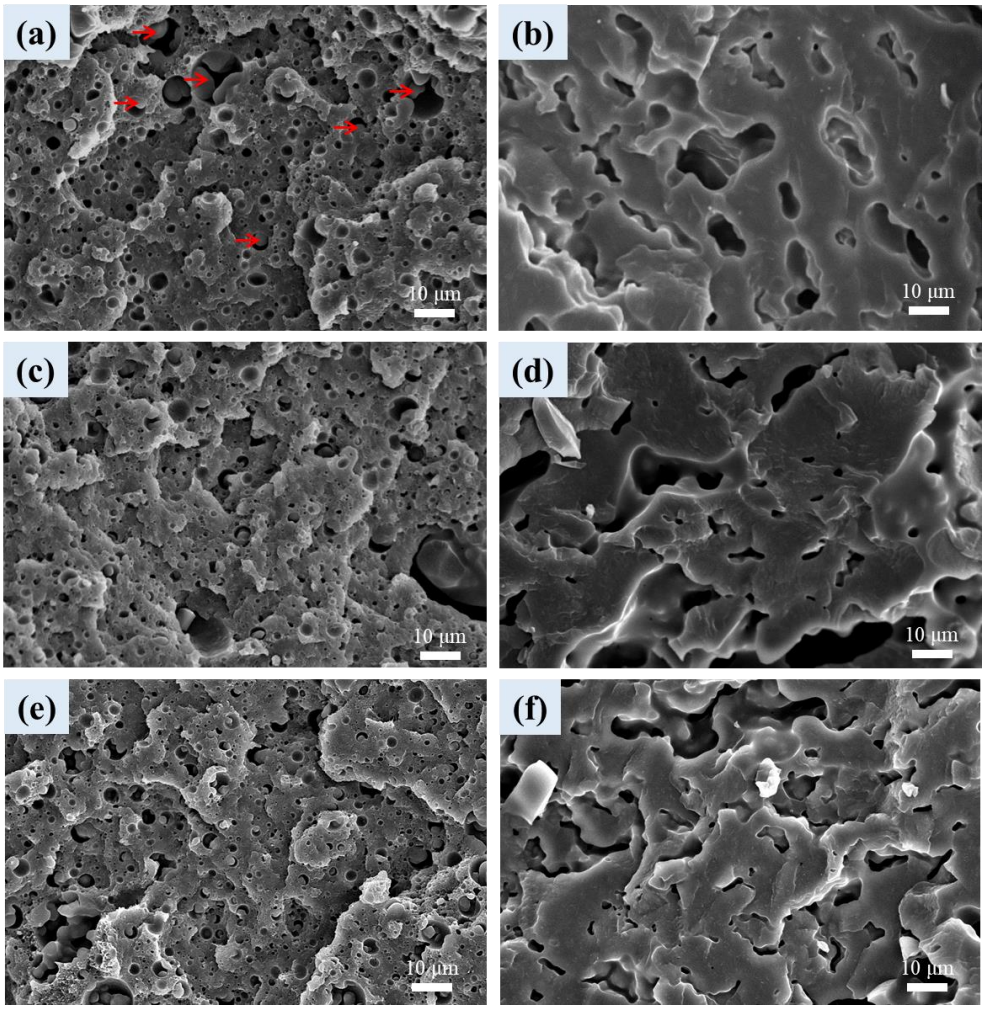



**Figure 8.** SEM cellular structure of (**a**) PLA(rich) phase in L1B1, (**b**) continuous PBAT phase in L1B1, (**c**) PLA(rich) phase in L1B1-T1, (**d**) continuous PBAT phase in L1B1-T1, (**e**) PLA(rich) phase in L1B1-C1, and (**f**) continuous PBAT phase in L1B1-C1.

For the L1B3 blend and composites of Figure 9, irregular/elongated shaped cells in the PBAT matrix were observed. The cells in composites (Figure 9b,c) were generally smaller than those observed in parent L1B3 foam (Figure 9a), which was again caused by the CNT- or CB-induced cell nucleation during foaming. The cell density was higher in the composites compared with their parent blend. A few large cells (not nucleated by the CNTs/CBs) also showed up in the PBAT matrix of the composites (surrounded by a dashed line). The average cell size and porosity of the foamed samples are summarized in Table 3. In this regard, techniques such as improving the miscibility between PLA and PBAT or inducing the branching/crosslinking of PBAT chains in samples are feasible to modify the irregularities of the PBAT cell structure.

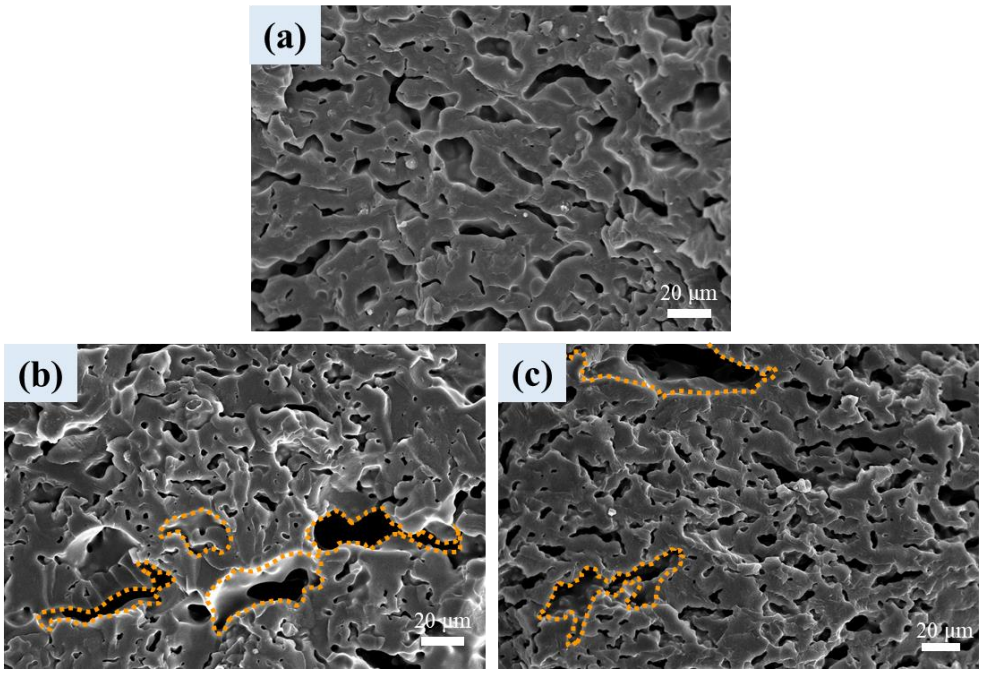



**Figure 9.** SEM cellular structure of PBAT phase in (**a**) L1B3, (**b**) L1B3-T1, and (**c**) L1B3-C1.

### *3.7. Melting Behavior of Foamed Samples*

Foaming selectively occurred in the PBAT phase of the samples. The DSC melting behavior of PBAT in the $scCO_2$-treated/untreated representative samples is compared in Figure 10. The results of the L3B1 system were not shown due to the low content of PBAT. Figure 10a compares the heating curves of $scCO_2$-treated and untreated PBAT. The original single broad endotherm of untreated PBAT evolved into a low-temperature broad endotherm (ca. 80–120 °C) and a high-temperature melting peak (arrowed, around 142 °C) after the $scCO_2$ treatment. The melting behavior modification indicates that the $scCO_2$ treatment must have aligned some PBAT chains in a perfect/thick lamellar crystal state and also induced some thin lamellar crystals, leading to the stability of the bimodal crystals. The heating curves of treated/untreated L1B1 are depicted in Figure 10a. Similar to neat PBAT, high-temperature, and low-temperature melting endotherms of PBAT crystals were observed in foamed L1B1. In addition, the PLA cold crystallization, which existed in untreated L1B1, was not observed after the $scCO_2$ treatment and showed a slightly higher temperature ($T_{Lm}$) melting peak of PLA compared with the untreated counterpart. These observations demonstrated that PLA cold crystallization was facilitated and occurred during the $scCO_2$ treatment, and more perfect PLA crystals were grown compared with the cold-crystallized PLA crystals in the untreated sample. For the representative $scCO_2$-treated L1B1- and L1B3-based composites, the modification in PBAT melting behavior similar to those of treated PBAT and L1B1 was also observed (Figure 10b). The melting endotherm of PBAT increased as its content increased in the composites. The disappearance of PLA cold crystallization and the rise in PLA melting temperature were again observed in the treated composites.

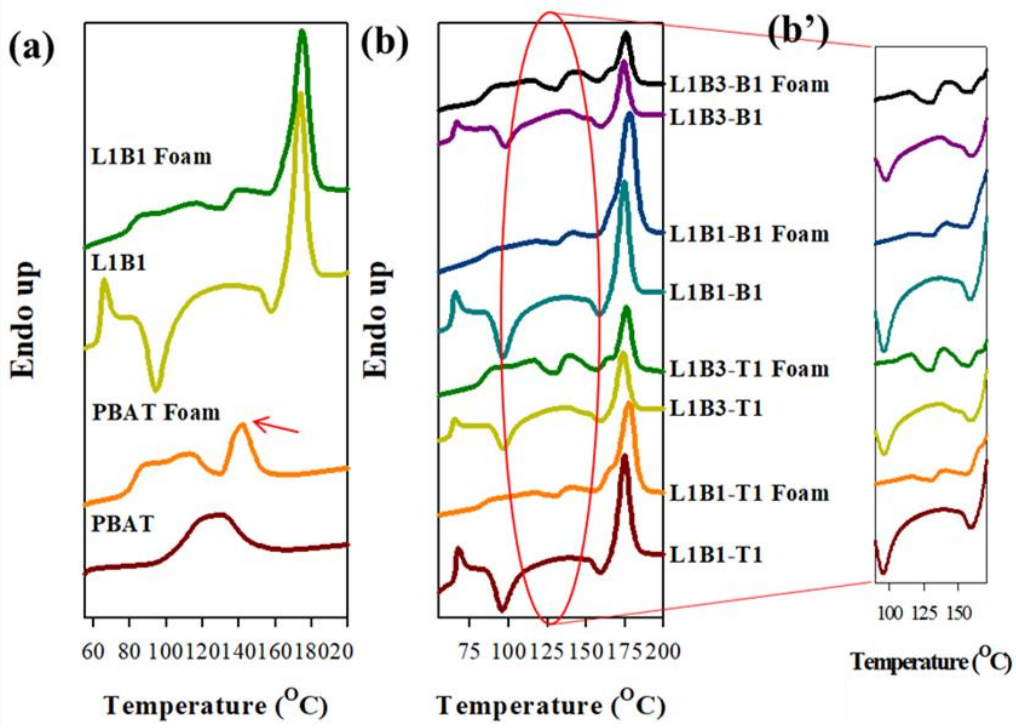



**Figure 10.** DSC 20 °C/min-heating curves of samples w/o $scCO_2$-treatment (foaming): (**a**) PBAT and L1B1 and (**b**,**b'**) L1B1- and L1B3-based composites.

### *3.8. Hardness of Unfoamed/Foamed Samples*

The rigidity-associated hardness of the prepared samples was measured, and the values are recorded in Table 4. Neat PLA possessed a higher hardness than that of neat PBAT (82 vs. 51), confirming the more rigid characteristic of PLA. The blend with higher PLA content possessed a higher hardness value. The addition of 1 phr rigid CNTs or CBs slightly increased the hardness of the parent blends. Regarding the foamed samples, the hardness declined compared with their unfoamed counterparts. The formation of cellular structure in the PBAT phase was responsible for the decrease in hardness.

**Table 4.** Hardness data of prepared samples.

| | **Samples** | | | | | |
|---|---|---|---|---|---|---|
| | **PLA** | **PBAT** | **PBAT Foam** | | | |
| Hardness | 82 | 51 | 40 | | | |
| | L3B1 | L3B1 foam | L3B1-T1 | L3B1-T1 foam | L3B1-B1 | L3B1-B1 foam |
| Hardness | 71 | 60 | 73 | 61 | 72 | 63 |
| | L1B1 | L1B1 foam | L1B1-T1 | L1B1-T1 foam | L1B1-B1 | L1B1-B1 foam |
| Hardness | 61 | 53 | 62 | 55 | 63 | 58 |
| | L1B3 | L1B3 foam | L1B3-T1 | L1B3-T1 foam | L1B3-B1 | L1B3-B1 foam |
| Hardness | 53 | 41 | 55 | 43 | 54 | 43 |

## 4. Conclusions

In this study, a twin-screw extruder was used to fabricate PLA/PBAT blends and blend-based nanocomposites with CNT or CB inclusion. Neat components and prepared blends/composites were further treated with $scCO_2$ to prepare samples selectively foamed in the PBAT phase. SEM results confirmed the immiscible characteristic of the blends, and a (quasi)co-continuous phase morphology was developed in the L1B1 blend. The added CNTs or CBs were selectively distributed in the PBAT phase of the blend-based composites

and, thus, played as nucleation agents for PBAT crystallization in different composites. The thermal stability of the PBAT portion in different composites was slightly improved due to the selective dispersion of CNTs/CBs in the PBAT phase. Compared with the parent blends, the electrical resistivity decreased by more than six orders of magnitude for L1B1- and L1B3-based composites, confirming the formation of double percolation phase morphology of PBAT-CNT/CB phase in the composites. After the $scCO_2$ treatment under a designed condition, selective foaming in the PBAT phase of the blends and composites was observed. The cellular structure of the PBAT phase in the blends was similar to the size/shape of PBAT domains in the untreated blends or the cellular structure in the neat PBAT foam, which suggested the PLA counterpart was hardly involved in the foaming process. The presence of CNTs or CBs in the composites slightly reduced the cell size of the foamed PBAT phase due to the CNT/CB-induced cell nucleation. The $scCO_2$ treatment induced the growth of the bimodal stability of PBAT crystals (two groups of lamellar thickness) in different samples, and PBAT melted mainly in two temperature regions. The hardness of the blends increased with increasing PLA content and slightly increased after forming the rigid CNT/CB-added corresponding composites. The foamed samples showed lower hardness than the corresponding unfoamed samples.

**Supplementary Materials:** The following supporting information can be downloaded at: https://www.mdpi.com/article/10.3390/polym16141971/s1, Figure S1: Typical stress-strain curves of unfoamed samples.

**Author Contributions:** Conceptualization F.-C.C.; investigation, K.B. and X.-B.L.; methodology, K.B. and X.-B.L.; software, C.-H.T.; data curation, X.-B.L., K.B. and C.-H.T.; formal analysis, K.B. and X.-B.L.; visualization, X.-B.L. and C.-H.T.; validation, K.B. and X.-B.L.; writing—original draft preparation, F.-C.C. and K.B.; resources, F.-C.C.; writing—review and editing, K.B. and F.-C.C.; supervision, F.-C.C.; project administration, F.-C.C.; funding acquisition, F.-C.C. All authors have read and agreed to the published version of the manuscript.

**Funding:** We gratefully acknowledge the financial support to carry out this research work from (1) Chang Gung Memorial Hospital (Taoyuan, Taiwan): CMRPD2M0272, (2) National Science and Technology Council (NSTC, Taiwan): NSTC 112-2221-E-182-002-MY3, and NSTC 112-2811-E-182-005-MY3. The authors also thank Yen-Hsiang Chang for funding and resources and the Microscopy Center at Chang Gung University for technical assistance.

**Institutional Review Board Statement:** Not applicable.

**Informed Consent Statement:** Not applicable.

**Data Availability Statement:** The data presented in this study are available on request.

**Conflicts of Interest:** The authors declare no conflicts of interest.

## References

1. Albano, C.; Reyes, J.; Ichazo, M.; Gonz´alez, J.; Brito, M.; Moronta, D. Analysis of the mechanical, thermal and morphological behaviour of polypropylene compounds with sisal fibre and wood flour, irradiated with gamma rays. *Polym. Degrad. Stab.* **2002**, *76*, 191–203. [CrossRef]
2. Tessanan, W.; Phinyocheep, P.; Amornsakchai, T. Sustainable materials with improved biodegradability and toughness from blends of poly(lactic acid), pineapple stem starch and modified natural rubber. *Polymers* **2024**, *16*, 232–254. [CrossRef] [PubMed]
3. Wang, L.; Abenojar, J.; Martínez, M.A.; Santiuste, C. Degradation of mechanical properties of flax/PLA composites in hygrothermal aging conditions. *Polymers* **2024**, *16*, 528–547. [CrossRef] [PubMed]
4. Behera, K.; Chang, Y.H.; Liu, C.Y.; Chiu, F.C. PMMA-driven morphology modification and dramatic improvement in ductility for PVDF/PLA blends. *Polymer* **2022**, *252*, 124930–124941. [CrossRef]
5. Benkraled, L.; Zennaki, A.; Zair, L.; Arabeche, K.; Berrayah, A.; Barrera, A.; Bouberka, Z.; Maschke, U. Effect of plasticization/annealing on thermal, dynamic mechanical, and rheological properties of poly(lactic acid). *Polymers* **2024**, *16*, 974–998. [CrossRef]
6. Xu, H.; Ke, L.; Tang, M.; Shang, H.; Zhang, Z.L.; Xu, W.; Fu, Y.N.; Wang, Y.; Tang, D.; Huang, D.; et al. Pea pod-mimicking hydroxyapatite nanowhisker-reinforced poly(lactic acid) composites with bone-like strength. *Int. J. Biol. Macromol.* **2022**, *216*, 114–123. [CrossRef]

7. Kuboki, T. Mechanical properties and foaming behavior of injection molded cellulose fiber reinforced polypropylene composite foams. *J. Cell. Plast.* **2014**, *50*, 129–143. [CrossRef]
8. Wang, L.; Hikima, Y.; Ohshima, M.; Yusa, A.; Yamamoto, S.; Goto, H. Development of a simplified foam injection molding technique and its application to the production of high void fraction polypropylene foams. *Ind. Eng. Chem. Res.* **2017**, *56*, 13734–13742. [CrossRef]
9. Zhao, B.; Hamidinejad, M.; Wang, S.; Bai, P.W.; Che, R.C.; Zhang, R.; Park, C.B. Advances in electromagnetic shielding properties of composite foams. *J. Mater. Chem. A* **2021**, *14*, 8896–8949. [CrossRef]
10. Nofar, M.; Park, C.B. Poly(lactic acid) foaming. *Prog. Polym. Sci.* **2014**, *39*, 1721–1741. [CrossRef]
11. Li, M.; Li, S.; Liu, B.; Jiang, T.; Zhang, D.; Cao, L.; He, L.; Gong, W. Rheological behavior, crystallization properties, and foaming performance of chain-extended poly(lactic acid) by functionalized epoxy. *RSC Adv.* **2021**, *11*, 32799–32809. [CrossRef] [PubMed]
12. Hamad, K.; Kaseem, M.; Ayyoob, M.; Joo, J.; Deri, F. Polylactic acid blends: The future of green, light and tough. *Prog. Polym. Sci.* **2018**, *85*, 83–127. [CrossRef]
13. Xu, H.; Zhou, J.; Odelius, K.; Guo, Z.; Guan, X.; Hakkarainen, M. Nanostructured phase morphology of a biobased copolymer for tough and UV-resistant polylactide. *ACS Appl. Polym. Mater.* **2021**, *3*, 1973–1982. [CrossRef]
14. Behera, K.; Chang, Y.H.; Yadav, M.; Chiu, F.C. Enhanced thermal stability, toughness, and electrical conductivity of carbon nanotube-reinforced biodegradable poly(lactic acid)/poly(ethylene oxide) blend-based nanocomposites. *Polymer* **2020**, *186*, 122002–122014. [CrossRef]
15. Fan, Z.; Gao, J.; Wu, Y.; Yin, D.; Chen, S.; Tu, H.; Wei, T.; Zhang, C.; Zhu, H.; Jin, H. Highly enhanced mechanical, thermal, and crystallization performance of PLA/PBS composite by glass fiber coupling agent modification. *Polymers* **2023**, *15*, 3164–3182. [CrossRef] [PubMed]
16. Boruvka, M.; Base, R.; Novak, J.; Brdlik, P.; Behalek, L.; Ngaowthong, C. Phase morphology and mechanical properties of super-tough PLLA/TPE/EMA-GMA ternary blends. *Polymers* **2024**, *16*, 192–212. [CrossRef] [PubMed]
17. Al-Tamimi, A.; Pandžić, A.; Kadrić, E. Investigation and prediction of tensile, flexural, and compressive properties of tough PLA material using definitive screening design. *Polymers* **2023**, *15*, 4169–4186. [CrossRef] [PubMed]
18. Sun, D.; Gu, T.; Qi, X.; Yang, J.; Lei, Y.; Wang, Y. Highly-toughened biodegradable poly(L-lactic acid) composites with heat resistance and mechanical-damage-healing ability by adding poly(butylene adipate-co-butylene terephthalate) and carbon nanofibers. *Chem. Eng. J.* **2021**, *424*, 130558–130571. [CrossRef]
19. Wang, X.; Peng, S.; Chen, H.; Yu, X.; Zhao, X. Mechanical properties, rheological behaviors, and phase morphologies of high-toughness PLA/PBAT blends by in-situ reactive compatibilization. *Compos. Part B* **2019**, *173*, 107028–107038. [CrossRef]
20. Wu, N.; Zhang, H. Mechanical properties and phase morphology of super-tough PLA/PBAT/EMA-GMA multicomponent blends. *Mater. Lett.* **2017**, *192*, 17–20. [CrossRef]
21. Liu, W.; Chen, P.; Wang, X.D.; Wang, F.C.; Wu, Y.J. Effects of poly(butyleneadipate-co-terephthalate) as a macromolecular nucleating agent on the crystallization and foaming behavior of biodegradable poly(lactic acid). *Cell. Polym.* **2017**, *36*, 75–96. [CrossRef]
22. Masiuchok, O.; Iurzhenko, M.; Kolisnyk, R.; Mamunya, Y.; Godzierz, M.; Demchenko, V.; Yermolenko, D.; Shadrin, A. Polylactide/carbon black segregated composites for 3D printing of conductive products. *Polymers* **2022**, *14*, 4022–4040. [CrossRef] [PubMed]
23. Alosime, E.M.; Basfar, A.A. A systematic investigation on the effect of carbon nanotubes and carbon black on the mechanical and flame retardancy properties of polyolefin blends. *Polymers* **2024**, *16*, 417–436. [CrossRef] [PubMed]
24. Behera, K.; Veluri, S.; Chang, Y.H.; Yadav, M.; Chiu, F.C. Nanofillers-induced modifications in microstructure and properties of PBAT/PP blend: Enhanced rigidity, heat resistance, and electrical conductivity. *Polymer* **2020**, *203*, 122578–122590. [CrossRef]
25. Jen, T.N.; Behera, K.; Chang, Y.H.; Chiu, F.C. Improving the ductility, toughness, and electrical conductivity of poly(lactic acid) by forming poly(lactic acid)/thermoplastic polyester elastomer blend and blend-based nanocomposites. *Polym. Compos.* **2022**, *44*, 1–11. [CrossRef]
26. Soni, S.K.; Thomas, B.; Thomas, S.B.; Tile, P.S.; Sakharwade, S.G. Carbon nanotubes as exceptional nanofillers in polymer and polymer/fiber nanocomposites: An extensive review. *Mater. Today Commun.* **2023**, *37*, 107358–107390. [CrossRef]
27. Urquijoa, J.; Aranburua, N.; Dagréoub, S.; Guerrica-Echevarríaa, G.; Eguiazábala, J.I. CNT-induced morphology and its effect on properties in PLA/PBAT-based nanocomposites. *Eur. Polym. J.* **2017**, *93*, 545–555. [CrossRef]
28. Najafi, N.; Heuzey, M.C.; Carreau, P.J.; Therriault, D.; Park, C.B. Mechanical and morphological properties of injection molded linear and branched-polylactide (PLA) nanocomposite foams. *Eur. Polym. J.* **2015**, *73*, 455–465. [CrossRef]
29. Livi, S.; Lins, L.C.; Sar, G.; Gerard, J.F.; Rumeau, J.D. Supercritical $CO_2$−Ionic liquids: A successful wedding to prepare biopolymer foams. *ACS Sustain. Chem. Eng.* **2016**, *4*, 461–470. [CrossRef]
30. Lee, R.E.; Azdast, T.; Wang, G.; Wang, X.; Lee, P.C.; Park, C.B. Highly expanded finecell foam of polylactide/polyhydroxyalkanoate/nano-fibrillated polytetrafluoroethylene composites blown with mold-opening injection molding. *Int. J. Biol. Macromol.* **2020**, *155*, 286–292. [CrossRef]
31. Li, Y.; Yin, D.; Liu, W.; Zhou, H.; Zhang, Y.; Wang, X. Fabrication of biodegradable poly(lactic acid)/carbon nanotube nanocomposite foams: Significant improvement on rheological property and foamability. *Int. J. Biol. Macromol.* **2020**, *163*, 1175–1186. [CrossRef] [PubMed]

32. Li, B.; Zhao, G.; Wang, G.; Zhang, L.; Gong, J.; Shi, Z. Biodegradable PLA/PBS open-cell foam fabricated by supercritical $CO_2$ foaming for selective oil-adsorption. *Sep. Purif. Technol.* **2021**, *257*, 117949–117959. [CrossRef]
33. Behera, K.; Chang, Y.H.; Chiu, F.C. Manufacturing poly(butylene adipate-*co*-terephthalate)/high density polyethylene blend-based nanocomposites with enhanced burning anti-dripping and physical properties—Effects of carbon nanofillers addition. *Compos. Part B Eng.* **2021**, *217*, 108878–108889. [CrossRef]

**Disclaimer/Publisher's Note:** The statements, opinions and data contained in all publications are solely those of the individual author(s) and contributor(s) and not of MDPI and/or the editor(s). MDPI and/or the editor(s) disclaim responsibility for any injury to people or property resulting from any ideas, methods, instructions or products referred to in the content.